N O T I C E

THIS DOCUMENT HAS BEEN REPRODUCED FROM MICROFICHE. ALTHOUGH IT IS RECOGNIZED THAT CERTAIN PORTIONS ARE ILLEGIBLE, IT IS BEING RELEASED IN THE INTEREST OF MAKING AVAILABLE AS MUCH INFORMATION AS POSSIBLE

NASA Technical Memorandum 81410

COMPUTATION OF THREE-DIMENSIONAL FLOW IN TURBOFAN MIXERS AND COMPARISON WITH EXPERIMENTAL DATA

L. A. Povinelli, B. H. Anderson,
and W. Gerstenmaier
Lewis Research Center
Cleveland, Ohio

Prepared for the
Eighteenth Aerospace Sciences Meeting
sponsored by the American Institute of Aeronautics and Astronautics
Pasadena, California, January 14-16, 1980

COMPUTATION OF THREE-DIMENSIONAL FLOW IN TURBOFAN MIXERS AND COMPARISON WITH EXPERIMENTAL DATA

Louis A. Povinelli*, B. H. Anderson**, and W. Gerstenmaier***
National Aeronautics and Space Administration
Lewis Research Center
Cleveland, Ohio 44135

Abstract

A three-dimensional, viscous computer code was used to calculate the mixing downstream of a typical turbofan mixer geometry. Experimental data were obtained using pressure and temperature rakes at the lobe and nozzle exit stations. Secondary flow velocities were also obtained. These data were used to validate the computer results. An assessment was also made to determine the relative importance of turbulence in the mixing phenomenon as compared with the streamwise vorticity setup by the secondary flows. The observations suggest that the generation of streamwise vorticity appears to play a significant role in determining the temperature distribution at the nozzle exit plane.

Nomenclature

E	energy
h	metric coefficient
i	unit vector
Pr	Prandtl number
Q	magnitude of $\bar{U}$, equal to $(u^2 + v^2 + w^2)$
Re	Reynolds number
$\bar{U}$	velocity vector
u	primary velocity
v,w	secondary velocities
x,y,z	three component directions
γ	specific heat ratio
μ	viscosity
ξ	vorticity
ρ	density
ϕ	velocity potential
ψ	stream function
Subscripts:	
I	inviscid component
p	primary component
s	secondary component
T	turbulent
v	viscous component
ϕ	irrotational component
ψ	rotation
1,2,3	components in x,y,z direction

*Aeronautical Research Engineer, Associate Fellow AIAA.

**Head, Aerodynamic Analysis Section, Member AIAA.

***Aeronautical Research Engineer.

Introduction

Turbofan forced mixer nozzles have been studied extensively as a means of improving fuel efficiency and providing jet noise reduction by reducing nozzle exit velocity. In the lobed mixer nozzle, the hot core flow passes up through the lobed section and the cooler fan flow passes down through the valleys (fig. 1). Very simply, these nozzles increase mixing by providing a much greater interface between the hot core flow and cooler fan flow. By mixing the core and fan flow in this manner, a small but significant performance gain can be realized. The level of gain depends on the trade-offs between the degree of mixing of the two streams and the viscous losses incurred in the mixing process.

Three-dimensional viscous analysis has been used by Birch, Paynter, Spalding, and Tatchell[1] to investigate the mixing process within turbofan engine exhaust nozzles with good results. It was suggested, however, that the discrepancy between prediction and measurement may be due in part to the turbulence model and to the uncertainty in the initial conditions. In addition, it was also concluded that the calculations were sensitive to initial boundary layer thickness on the plug. In the Aeropropulsion 1979 Conference[2] held at Lewis Research Center it was further suggested that the secondary flows may also play an important role in the mixing process within engine exhaust nozzles. Calculations were presented based on the analysis of Kreskovsky, Briley, and McDonald[3] that streamwise vorticity, which is a measure of the degree of secondary flow, can be enhanced within the mixer nozzle due to transverse pressure gradients, arising from the plug shape.[2] This suggests that three elements affect the turbulent mixing process, that is, (1) the turbulent transport process, (2) the streamwise vorticity at entry, and (3) induced secondary flow within the mixing duct itself.

To further investigate and illuminate the physical processes that can be important within forced mixer nozzles, and to explain the large differences in mixing with relatively small lobe geometry changes, an experimental and analytical effort was initiated. This paper describes some initial results of this effort.

Governing Equations

In this study, the forced mixer flow field is computed by a spatial marching method which solves the simplified form of the three-dimensional NS equations.[3-5] A curvilinear orthogonal coordinate system is used with coordinate directions x,y,z and corresponding metric coefficients h_1,h_2,h_3. Here x is defined as the streamwise marching direction and y and z are the two crossflow directions. In order to allow the use of a marching procedure, x-direction diffusion terms have been neglected. The solution method centers around the decomposition of the velocity into primary and secondary flow components

$$\bar{U} = \bar{U}_p + \bar{U}_s$$

The equation governing development of the primary velocity component is

$$\rho u h_2 h_3 \frac{\partial u}{\partial x} + \rho(v_s) h_1 h_3 \frac{\partial u}{\partial y} + \rho(w_s) h_1 h_2 \frac{\partial u}{\partial z} + \rho(v_s) u h_3 \frac{\partial h_1}{\partial y} - \rho(v_s)^2 h_3 \frac{\partial h_2}{\partial x} - \rho(w_s)^2 h_2 \frac{\partial h_3}{\partial x} + h_2 h_3 \frac{\partial p_I}{\partial x} + h_2 h_3 \frac{dp_V(x)}{dx} = \frac{1}{Re} \frac{\partial}{\partial y}\left[\frac{(\mu+\mu_T) h_1 h_3}{h_2} \frac{\partial u}{\partial y}\right] + \frac{h_1 h_2}{Re h_3} \frac{\partial}{\partial z}\left[\frac{(\mu+\mu_T)\partial u}{\partial z}\right]$$

where U represents the sole component of $\bar{U}_p$, p_I the imposed pressure and $P_V(x)$ represents the main viscous pressure drop which is determined from the mass flux condition

$$\iint_A h_2 h_3 \rho u dy dz = C$$

To account for thermal mixing between the fan and core streams, an energy equation is introduced in the form

$$\rho u h_2 h_3 \frac{\partial E}{\partial x} + \rho(v_s) h_1 h_3 \frac{\partial E}{\partial y} + \rho(w_s) h_1 h_2 \frac{\partial E}{\partial z} = \frac{1}{Re} \frac{\partial}{\partial y}\left[\left(\frac{\mu}{Pr} + \frac{\mu_T}{Pr_T}\right) \frac{h_1 h_3}{h_2} \frac{\partial E}{\partial y} + \frac{h_1 h_3}{2h_2}\left(\mu + \mu_T - \frac{\mu}{Pr} - \frac{\mu_T}{Pr_T}\right) \frac{\partial}{\partial y}(\bar{U}^2 + \bar{W}_s^2)\right] + \frac{1}{Re} \frac{h_1 h_2}{h_3} \frac{\partial}{\partial z}\left[\left(\frac{\mu}{Pr} + \frac{\mu_T}{Pr_T}\right) \frac{\partial E}{\partial z} + 1/2 \left(\mu + \mu_T - \frac{\mu}{Pr} - \frac{\mu_T}{Pr_T}\right) \frac{\partial}{\partial z}(\bar{U}^2 + \bar{V}^2)\right]$$

The gas law is then introduced in the form

$$\frac{\partial}{\partial x}\left[\left(\frac{\gamma-1}{\gamma}\right)\rho\left(E - \frac{u^2}{2}\right)\right] = \frac{\partial P_I}{\partial x} + \frac{dP_V(x)}{dx}$$

which relates the imposed and viscous pressure gradients to the other dependent variables.

To determine the secondary velocity, $\bar{U}_S$ is assumed to consist of an irrotational and rotational component. The rotational components of $\bar{U}_S$ are determined from solution of a streamwise vorticity equation of the form

$$\frac{u}{Q}\left(\rho u \frac{\partial \xi}{\partial y} - \xi \frac{\partial \rho u}{\partial x}\right) + \frac{v_s}{Q} \frac{h_1}{h_2}\left(\rho u \frac{\partial \xi}{\partial y} - \xi \frac{\partial \rho u}{\partial y}\right) + \frac{w_s}{Q} \frac{h_1}{h_3}\left(\rho u \frac{\partial \xi}{\partial z} - \xi \frac{\partial \rho u}{\partial z}\right) = -\frac{2}{h_2} \frac{\partial h_1}{\partial y} \rho u \frac{1}{h_3} \frac{\partial u}{\partial z} - \frac{h_1}{h_2 h_3} \frac{1}{\rho}\left[\frac{\partial P}{\partial y} \frac{\partial \rho}{\partial z} - \frac{\partial \rho}{\partial y} \frac{\partial P}{\partial z}\right] + \frac{\rho}{Re}\left\{\frac{h_1}{h_2 h_3} \frac{\partial}{\partial y}\left[\frac{h_3}{h_1 h_2 \rho} \frac{\partial h_1(\mu+\mu_T)\xi}{\partial y}\right] + \frac{h_1}{h_3^2} \frac{\partial}{\partial z}\left[\frac{1}{\rho} \frac{\partial(\mu+\mu_T)\xi}{\partial z}\right]\right\}$$

where

$$Q^2 = u^2 + v_s^2 + w_s^2$$

and the vorticity is assumed to lie in the transverse coordinate surface and is defined by

$$\xi = \frac{1}{h_2 h_3}\left(\frac{\partial h_3 w_s}{\partial y} - \frac{\partial h_2 v_s}{\partial z}\right)$$

Once a solution for vorticity is obtained, a vector potential is determined from the equation

$$\frac{1}{h_2 h_3} \frac{\partial}{\partial y}\left[\left(\frac{h_3}{\rho h_1 h_2}\right) \frac{\partial(h_1 \psi_s)}{\partial y}\right] + \frac{1}{h_1 h_3^2} \frac{\partial}{\partial z}\left[\left(\frac{1}{\rho}\right) \frac{\partial(h_1 \psi_s)}{\partial z}\right] = -\xi$$

The rotational components of the secondary flow are thus determined from the expressions

$$v_\psi = \frac{1}{\rho h_1 h_3} \frac{\partial(h_1 \psi_s)}{\partial z}$$

$$w_\psi = -\frac{1}{\rho h_1 h_2} \frac{\partial(h_1 \psi_s)}{\partial y}$$

The resulting velocity field is then corrected to satisfy local continuity through the introduction of a scalar potential governed by the expression

$$\frac{\partial}{\partial y}\left[\frac{\rho h_1 h_3}{h_2} \frac{\partial \phi_s}{\partial y}\right] + \frac{\partial}{\partial z}\left[\frac{\rho h_1 h_2}{h_3} \frac{\partial \phi_s}{\partial z}\right] = -\frac{\partial(h_2 h_3 \rho u)}{\partial x}$$

The irrotational secondary velocity components can thus be determined from the equations

$$v_\phi = \frac{1}{h_2} \frac{\partial \phi_s}{\partial y}$$

$$w_\phi = \frac{1}{h_3} \frac{\partial \phi_s}{\partial z}$$

The secondary velocities are given by the sum of the rotational and irrotational components

$$v_s = v_\psi + v_\phi$$

$$w_s = w_\psi + w_\phi$$

and the vector velocity is given by

$$\bar{u} = \bar{i}_1 u_p + \bar{i}_2 v_s + \bar{i}_3 w_s$$

The turbulent viscosity is determined using the two equations K - ε turbulence model presented by Launder and Spalding.(6)

The governing equations were applied to the general geometry shown in figure 1. The computational mesh starts at the lobe exit plane and the three-dimensional viscous solution is marched downstream. Although the mixer is axisymmetric, the

flow is three-dimensional due to azimuthal variation of the cold fan and hot core streams.

Experimental Setup

A photograph of the test apparatus is shown in figure 2. It consisted of a fixed upstream model section and a rotating shroud. Figure 3 shows a cutaway of the test apparatus. The mixer lobe section was interchangeable. The rotating shroud contained instrumentation rakes for probing the flow field. Total temperatures were measured at five stations in the mixing region. The first station was at the lobe exit plane, the second was halfway to the plug end, the third was at the end of the plug, the fourth was midway between the plug end and the nozzle exit, and the fifth station was at the nozzle exit plane. In addition, the temperatures and pressures were measured upstream for both the core and fan streams. The rotating mechanism can be seen in figure 2 as well as the rakes at the lobe exit and nozzle exit stations. Total pressures were also measured at the lobe and nozzle exit stations. Temperature data were taken over a 54-degree segment in 3 degree increments. A typical temperature contour was based on data for 18 angular positions and 14 radial positions for a total of 252 measurements. The ratio of the shroud length to the inside shroud diameter was 0.71 based on the values at the lobe exit plane.

The test matrix of mixer geometries is shown in figure 4. Penetration (ratio of lobe radius to shroud radius) and lobe number were varied while maintaining constant mixing perimeter. The spacing ratio, that is, the ratio of core-to-fan lobe included angles, was also changed in going from contour A to contours B and C. The two lower contours on the plot (A and C) were designed following current mixer trends. Model B was designed with a more gentle curvature on the upper core shape so as to avoid local separation. Only some of the data obtained with contours A and B will be presented.

The fan and core streams were operated with a total pressure ratio of unity and a total temperature ratio of 1.35. The Mach number of the fan and core streams at the mixing plane (lobe exit) was approximately 0.45 and the by-pass ratio was 4.

Calculated Results

A. Temperature and Vorticity

The computer program described was used to make a sample calculation of the mixing process and to evaluate the program in its present state of development. The starting condition for the calculation was a uniform flow that was aligned with the computational mesh shown in figure 1. No vorticity or secondary flow was present at the start of the computation.

The Reynolds number, based on the hot-stream velocity and the shroud diameter, was 900; the Mach number at the inlet plane was 0.35 in both streams and the temperature ratio was 2. The pie-shaped segment shown in figure 1, covering a half-lobe and fan trough, was used for the computational domain. Symmetry was assumed for the remainder of the geometry. The computational mesh within this segment was composed of 20 radial points and 10 circumferential. A dividing streamline was used at the plug base since the viscous marching method will not compute through a separated flow region. A few of the computed properties have been chosen for presentation. Figure 5 shows the total temperature and streamwise vorticity. The sequence of the temperature vorticity patterns reveal some interesting features which occur during the mixing process. At the lobe exit plane, there is no streamwise vorticity and the total temperature pattern defines the lobe geometry. As the solution initially moves downstream, there is relatively little change in the total temperature. Vortices are generated on both sides of the radial interface between the core flow and the fan flow. As the solution progresses downstream, the vortices initially generated in the core flow dissipate and the fan vortex pair dominate. As the vortex pair intensify near the end of the plug, faster mixing appears to take place. The overall effect is to enhance mixing. The vortex intensity and resulting enhanced mixing are probably due to the curvature of the flow at the end of the plug. This suggests that the centerbody shape may be important to the mixing process. Downstream of the plug, the streamwise vorticity dissipates. The computed results show that streamwise vorticity, which was not present at the start of the calculations, is generated in the plug region of the mixing passage.

B. Comparison With 18 Lobe Mixer

Calculations were performed on an 18-lobe forced mixer nozzle configuration using a preliminary version of the analysis described which did not have the $K - \varepsilon$ turbulence model but rather a simple constant viscosity model. No secondary flows were present in the initial conditions for the computation. The computed total temperature contours at the nozzle exit are presented in figure 6(a) whereas equivalent experimental data are shown in figure 6(b). In spite of the simple turbulence model used in this calculation, there are remarkable similarities between the analysis and experiment. It is observed that the high temperature zone is present in both patterns, and that the cold fan flow extends between the hot regions, toward the center of the duct. The computed contours also begin to show a "pinching" effect on the hot zone similar to that existing in the experimental data. The lack of better agreement in the contours is probably due to the fact that the secondary flows present in the experimental data at the lobe exit have not been accounted for in the computation. On the other hand, the data show some asymmetry which is not possible with the analysis. In addition, the experimental pattern shows a hot region at the center of the duct which may be due to recirculation at the base of the plug and/or the presence of a hot layer on the plug surface. The calculation did not have an initial hot layer under the fan trough or a plug boundary layer; nor did it account for separation and recirculation at the end of the plug.

The deep radial penetration of the cold fan flow and the beginning of a temperature inversion was not predicted by the analysis. In addition, the predicted "hot spots" were at a lower radial position than the measurements and the general temperature patterns tended to be more elongated.

Improvements in the comparison of theory and experimental data are anticipated, based on the inclusion of an improved mixing model, and correct secondary flow starting conditions at the lobe exit

plane instead of the use of uniform mesh-aligned flow. Results presented in the following sections illustrate the importance of understanding the starting or inlet flow field.

Experimental Results

A. Comparison of 12A and 12B Mixers

Temperature data obtained with the 12-lobe mixers, with lobe configurations A and B are shown in figure 7. Four axial stations are shown, starting at the lobe exit plane (fig. 7(a)) and finishing at the nozzle exit plane (fig. 7(d)). The locations of the intermediate stations are given in the section on Experimental Apparatus. The major difference in contours A and B lies in the fact that the velocity vector at the lobe exit plane has an outward radial component and less of a tendency for flow separation. Contour B has a slightly larger penetration. These differences would not appear, at first glance, to be significant changes in geometry. However, as seen in the results, the B contour has greater penetration, the maximum temperature at the nozzle exit is significantly lower, and the temperature pattern is radically different.

B. Discussion on Observed Secondary Flows

Two significant features of the data in figure 7(d) can be observed. The first feature is related to the fact that temperature inversion has taken place, whereby the hot core flow has been displaced radially outward, and the resulting void filled by the cold fan flow. In order to model this phenomenon it is necessary to account for the secondary flows which enter the mixer passage, that is, flow components normal to the grid lines at the lobe exit plane. The second major feature is concerned with the distortion that takes place in the temperature contours. Strong secondary flows have distorted the 12B pattern, resulting in a horseshoe-shaped contour. These data strongly suggest that secondary flow, such as the vortices shown in figure 5, significantly contribute to the mixing process.

C. LDV Measurements

Measurements of the three velocity components have been carried out at UTRC using an LDV technique.[7] The measurements were made on a plane normal to the centerline of the mixer nozzle and relative to a cylindrical coordinate system. Secondary velocity vectors for the radial and azimuthal directions are presented in figure 8 for a position just downstream of the lobe exit plane. Measurements were made at five equally-spaced angular locations between the centerline of the fan stream and the centerline of the core stream. Radial inflow is observed in the fan regions and radial outflow in the core regions. These secondary flow data may explain the horseshoe-shaped temperature contours obtained with the lobe B geometry. The radial flow pattern is also consistent with the presence of a vortex aligned with the interface between the fan and core flows. Some evidence of swirl is also observed (fig. 8) at the plug surface. In addition, a small vortex pair could be embedded at the top of the core, although the data are sparse. These secondary flow vector measurements, along with the temperature contours presented in the previous section, present strong evidence for the existence of large magnitude secondary flow in mixers. Inclusion of these secondary flows, as starting conditions, will be necessary in order to improve the comparison between experiment and calculations. Prediction of the secondary flows generated within the lobe section is a more difficult problem which deserves future attention.

Conclusions

The computer program described in this paper has been used to predict the existence of large-scale secondary flow downstream of the lobe exit plane. This large-scale, or macro mixing, is believed to be an important mechanism in addition to the conventional turbulent shear mixing by which the energy exchange occurs in forced mixers. It is now believed that properly accounting for these secondary flows at the lobe exit plane, through the use of experimental data, will lead to good agreement betwen analysis and data. Experimental evidence for the presence of secondary flow has been found using LDV measurements and temperature data.

References

1. Birch, S. F., Paynter, G. C., Spalding, D. B., and Tatchell, D. G., "Numerical Modelling of Three-Dimensional Flows in Turbofan Engine Exhaust Nozzles," Journal of Aircraft, Vol. 15, No. 8, August 1978, pp. 489-496.

2. Bowditch, D. N., McNally, W. D., Anderson, B. H., Adamczyk, J. J., and Sokol, P. M., "Computational Fluid Mechanics of Internal Flow," NASA CP-2092, 1979, pp. 187-230.

3. Briley, W. R. and McDonald H., "Analysis and Computation of Viscous Subsonic Primary and Secondary Flows," AIAA Paper 79-1453, July 1979.

4. Kreskovsky, J. P., Briley, W. R., and McDonald, H., "Development of a Method for Computing Three-Dimensional Subsonic Turbulent Flows in Turbofan Lobe Mixers," Scientific Research Associates, Inc., Glastonbury, CT., R79-300006-F, November 1979.

5. McDonald, H. and Briley, W. R., "Computational Fluid Dynamic Aspects of Internal Flows," AIAA Paper 79-1445, 1979.

6. Launder, B. E. and Spalding, D. B., "The Numerical Computation of Turbulent Flows," Computer Methods in Applied Mechanics and Engineering, Vol. 3, March 1974, pp. 269-289.

7. Patterson, R. and Werle, M. J., "Turbofan Forced Mixer Flow Field," United Technologies Research Center, East Hartford, CT., UTRC R79-912924-24, July 1979.

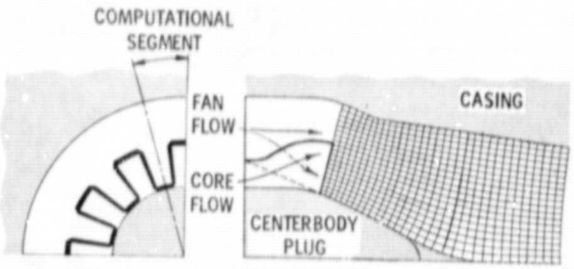

Figure 1. - Mixer nozzle solution mesh. C5-79-2170

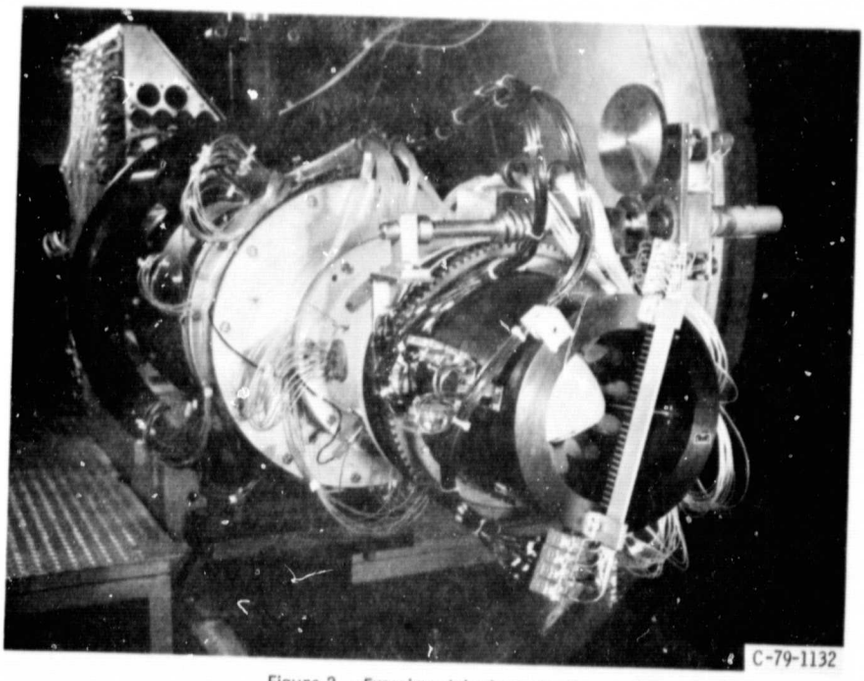

Figure 2. - Experimental mixer nozzle.

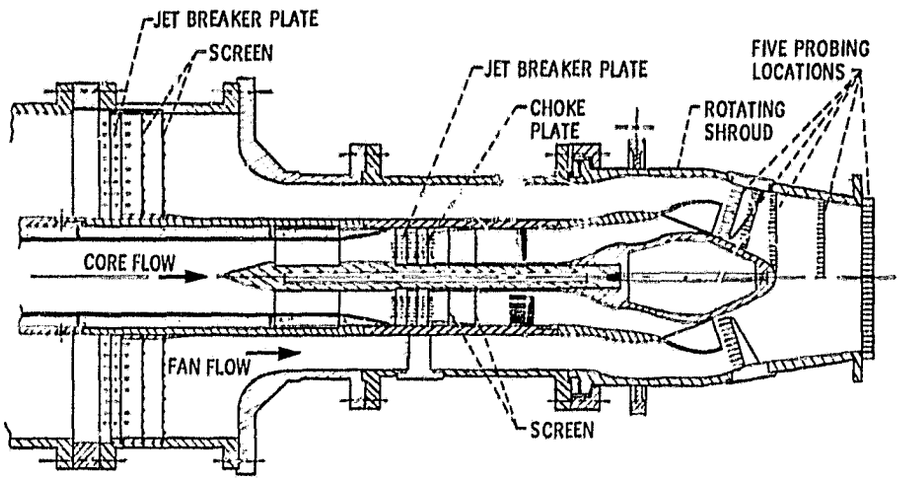

Figure 3. - Mixer nozzle model cross-section.

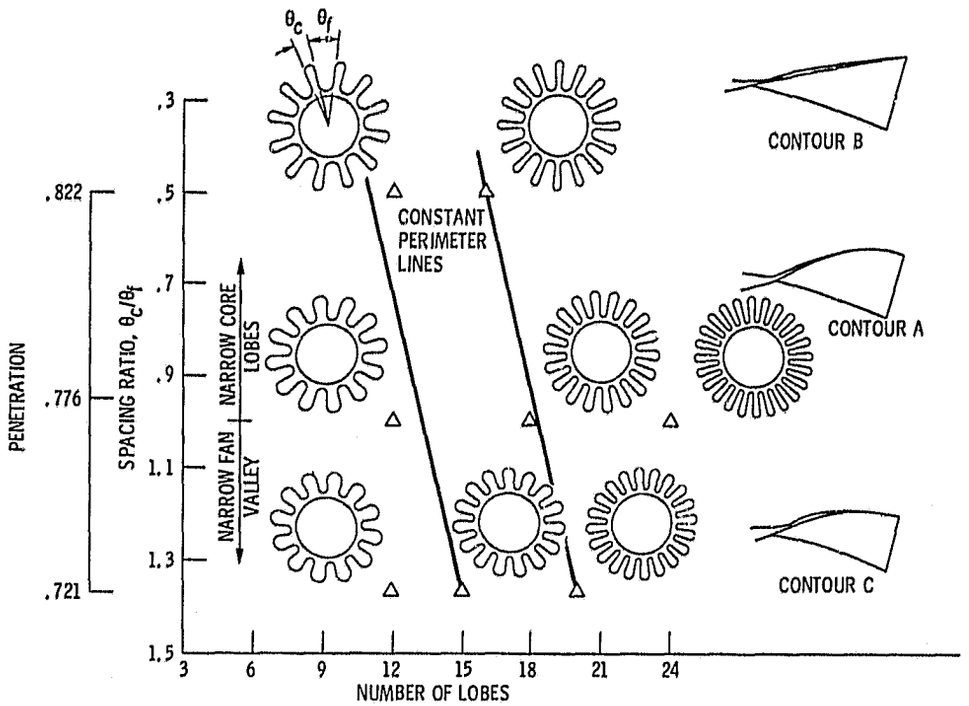

Figure 4. - Experimental test matrix, constant flow area.

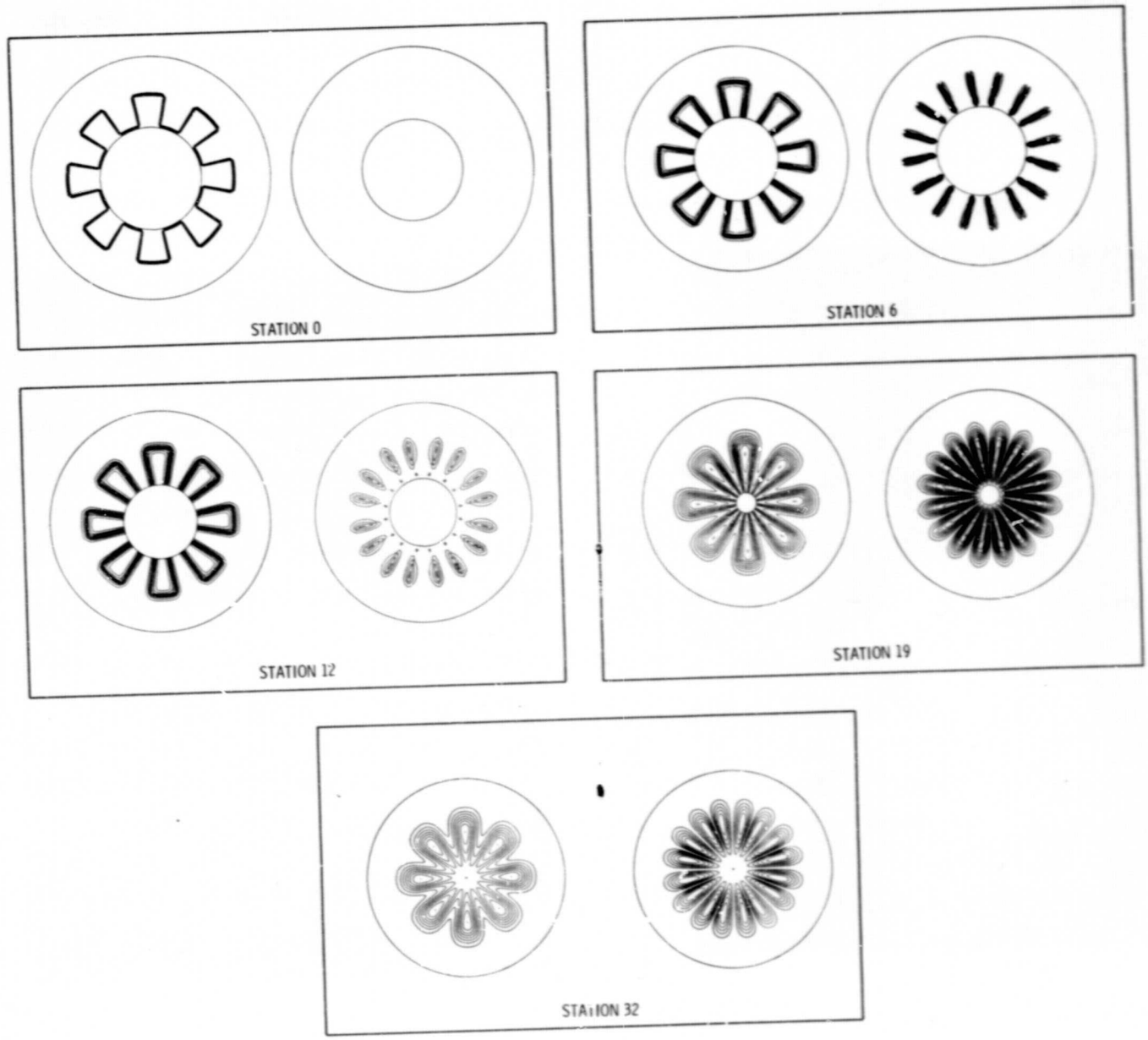

Figure 5. - Temperature and vorticity contours, computed.

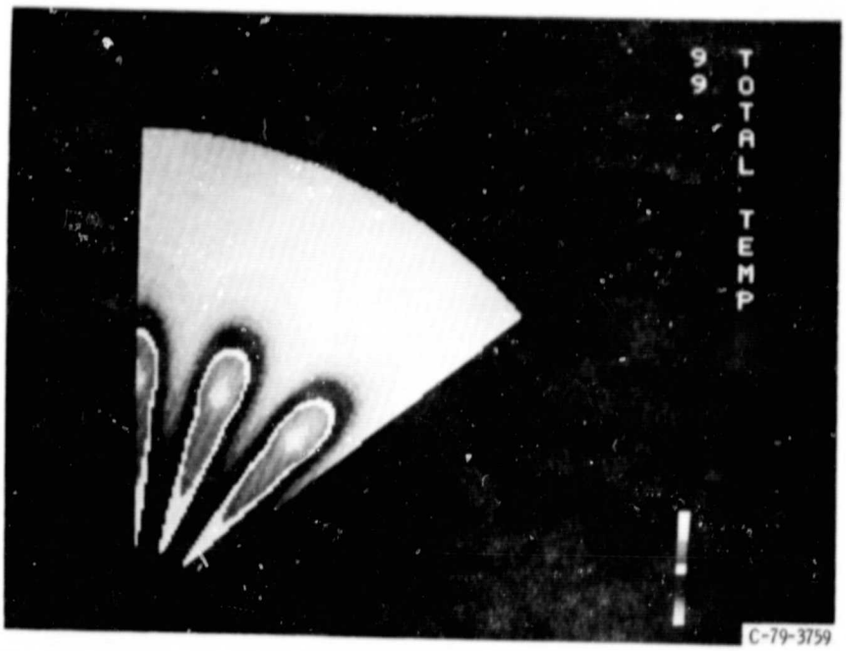

(a) COMPUTED RESULTS.

Figure 6. - Temperature contour for 18 lobe mixer.

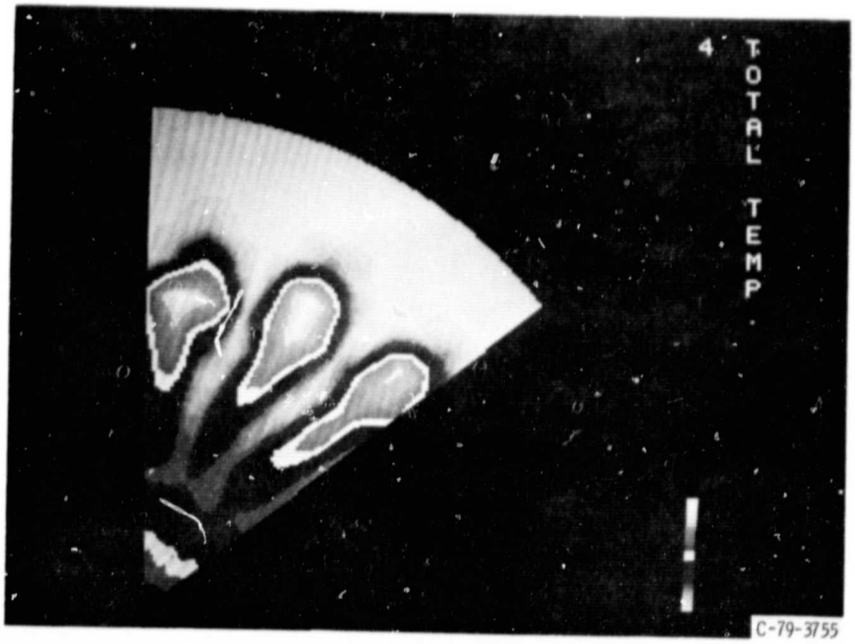

(b) EXPERIMENTAL RESULTS.

Figure 6. - Concluded.

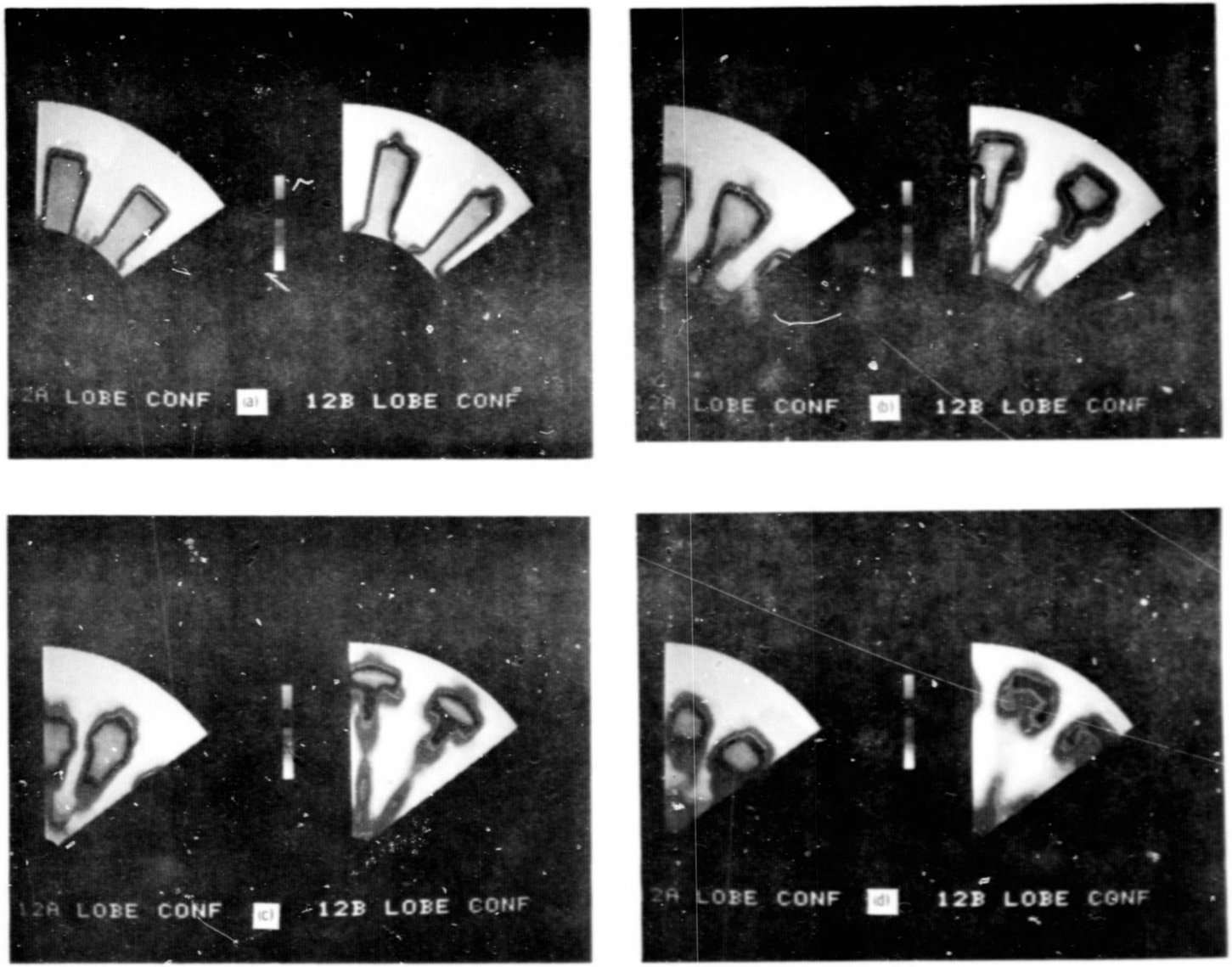

Figure 7. - LeRC experimental temperature contours - comparison of A and B configurations.

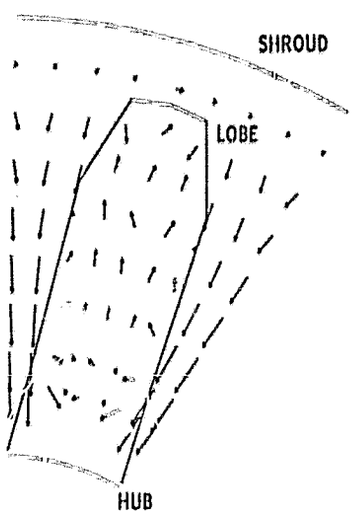

Figure 8. - LDV measurements of secondary velocities, lobe exit station.

1 Report No NASA TM-81410	2 Government Accession No	3 Recipient's Catalog No
4 Title and Subtitle COMPUTATION OF THREE-DIMENSIONAL FLOW IN TURBOFAN MIXERS AND COMPARISON WITH EXPERIMENTAL DATA		5 Report Date 6 Performing Organization Code
7 Author(s) L. A. Povinelli, B. H. Anderson, and W. Gerstenmaier		8 Performing Organization Report No E-324 10 Work Unit No
9 Performing Organization Name and Address National Aeronautics and Space Administration Lewis Research Center Cleveland, Ohio 44135		11 Contract or Grant No 13 Type of Report and Period Covered Technical Memorandum
12 Sponsoring Agency Name and Address National Aeronautics and Space Administration Washington, D.C. 20546		14 Sponsoring Agency Code

15 Supplementary Notes

16 Abstract

A three-dimensional, viscous computer code was used to calculate the mixing downstream of a typical turbofan mixer geometry. Experimental data were obtained using pressure and temperature rakes at the lobe and nozzle exit stations. Secondary flow velocities were also obtained. These data were used to validate the computer results. An assessment was also made to determine the relative importance of turbulence in the mixing phenomenon as compared with the streamwise vorticity setup by the secondary flows. The observations suggest that the generation of streamwise vorticity appears to play a significant role in determining the temperature distribution at the nozzle exit plane.

17. Key Words (Suggested by Author(s)) Mixers Nozzles Fuel efficiency Turbofan forced mixers	18. Distribution Statement Unclassified - unlimited STAR Category 34		
19. Security Classif. (of this report) Unclassified	20. Security Classif. (of this page) Unclassified	21. No. of Pages	22. Price*

* For sale by the National Technical Information Service, Springfield, Virginia 22161